ACS APPLIED ENERGY MATERIALS

www.acsaem.org Article

Facile Molecular Modification for Efficient and Stable Carbon-Based $CsPbI_3$ Perovskite Solar Cells

Zhixing Wang,[1] Jinqing Lv,[1] Weifeng Liu, Weiwei Sun, Zhiwen Dong, Kexiang Wang, Tingting You,* and Penggang Yin*

Cite This: https://doi.org/10.1021/acsaem.5c04098 Read Online

ACCESS | Metrics & More | Article Recommendations | Supporting Information

ABSTRACT: Carbon-based inorganic perovskite solar cells (C-IPSCs) with promising efficiency, good thermal stability, and low cost have emerged as important candidates for photovoltaic device commercialization. However, the relatively poor phase stability of $CsPbI_3$ perovskite in humid conditions and the mismatched energy level at the perovskite/carbon interface hinder the efficiency and stability of $CsPbI_3$ C-IPSCs. Herein, a facile molecular modification strategy is employed to solve the current issues using a multifunctional molecule, ethyl thioacetate (ES). Post-treatment enhances the hydrophobicity of $CsPbI_3$ films due to the relatively small polarity of ES molecules. The C═O and C−S groups in ES form Lewis acid−base coordination interactions with uncoordinated Pb^{2+} in perovskite, effectively passivating surface defects in perovskite films. In addition, ES treatment optimizes the energy level arrangement, facilitating hole extraction at the perovskite/carbon interface. Thus, ES post-treatment yields a champion PCE of 17.07% for carbon-based $CsPbI_3$ solar cells. The ES-treated C-IPSCs also show enhanced stability, which retains 80% of the initial PCE after 1360 h at 20% RH, surpassing the untreated counterparts by 19%.

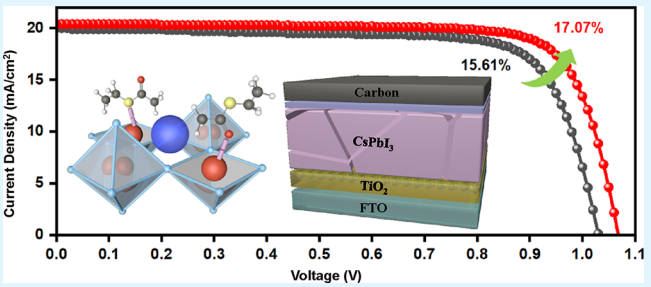

KEYWORDS: *inorganic perovskite, $CsPbI_3$, carbon electrode, molecular modification, high stability*

1. INTRODUCTION

As promising candidates for the next-generation photovoltaic devices, perovskite solar cells (PSCs) have a certified photovoltaic conversion efficiency (PCE) of over 27%.[1] The stability of PSCs is the main obstacle to their commercial application. This instability is mainly caused by organic cations including methylammonium (MA^+) and formamidine (FA^+), as well as the use of organic hole transport layers.[2] To address this issue, researchers have developed all inorganic perovskite by using Cs^+ to replace organic cations.[3−5] Meanwhile, to further reduce manufacturing costs and improve the stability of PSCs, many research works have used printable carbon electrodes to replace both hole transport layers and metal electrodes, which has led to higher device efficiency.[6] Therefore, inorganic PSCs based on carbon electrodes (C-IPSCs) with a device structure of FTO/electron transport layer/perovskite/carbon have attracted widespread attention in recent years.[7−9]

With relatively suitable bandgaps, $CsPbI_3$ C-IPSCs exhibit theoretically high PCE.[10−13] Xiang et al. developed a facile method to fabricate $CsPbI_3$ perovskite films with a broadened optical spectrum by replacing PbI_2 with $HPbI_3$ in dry air and achieved a PCE of 9.5% for C-IPSCs.[14] Wang et al. improved the crystal quality of the $CsPbI_3$ film by tuning the crystallization processes in dimethylammonium iodide (DMAI)-assisted $CsPbI_3$ perovskite films, thereby boosting the PCE of $CsPbI_3$ C-IPSCs to 14.6%.[15] Zhang et al. combined wet film treatment and dry film treatment to fabricate $CsPbI_3$ films with an in situ formed low-dimensional perovskite structure, which simultaneously passivated bulk and surface defects and achieved a PCE of 19.65% in C-IPSCs.[16]

Despite significant improvements in device efficiency, two major challenges persist for C-IPSCs: (1) the relatively poor phase stability of inorganic $CsPbI_3$ perovskite under a humid environment and (2) insufficient hole extraction at the inorganic perovskite/carbon interface. These factors continue to limit further advancements in both efficiency and stability. Various strategies have been proposed to solve the above-mentioned issues, including interface engineering,[17−19] component engineering,[20−22] and carbon electrode modification.[23−25] Interface engineering is a facile method to enhance the phase stability of inorganic perovskites and improve the energy level alignment between inorganic perovskites and

Received: December 27, 2025
Revised: February 20, 2026
Accepted: February 24, 2026

carbon electrodes. Zhang et al. constructed a 1D/3D heterostructure to passivate the defects of $CsPbI_3$ perovskite films and enhance its phase stability, thus achieving a new certified record of 17.8% for $CsPbI_3$ C-IPSCs.[26] Zhang et al. employed 4-trifluoromethyl-phenylammonium iodide at the perovskite/carbon interface to manipulate the dipole electric field. This strategy enhanced hole selectivity and charge separation at the interface, which in turn increased the PCE to 18.33%.[7] However, the above strategies have strict requirements for processing conditions and atmosphere, which undoubtedly increase the uncontrollability of the process. Therefore, developing simple postprocessing strategies with high process tolerance and a wide operational window is crucial for advancing the technology toward practical applications.

In this work, a facile molecular modification strategy using ethyl thioacetate (ES) is employed to simultaneously improve the phase stability of perovskites and the energy level alignment between perovskites and carbon electrodes. It is demonstrated that the carbonyl groups (C═O) and C−S in ES can form Lewis acid−base coordination interactions with uncoordinated Pb^{2+} in perovskite, passivating surface defects of $CsPbI_3$ perovskite films. In addition, ES treatment optimizes the energy level arrangement between inorganic perovskite and carbon electrodes, accelerating the hole extraction from inorganic perovskite to carbon electrodes. Thus, ES post-treatment yields a champion PCE of 17.07% for carbon-based $CsPbI_3$ solar cells with enhanced stability.

2. EXPERIMENTAL SECTION

2.1. Materials

S-Ethyl thioacetate (ES) was purchased from Aladdin. PbI_2 (99.99%) and CsI (99.99%) were from Xi'an Polymer Light Technology Corporation (China); $PbBr_2$ (99.999%) and isopropanol (IPA, 99.5%) were from J&K. Dimethylammonium iodide (DMAI, 99.9%) was from Advanced Election Technology Co., Ltd. Titanium diisopropoxide bis(acetylacetonate) (75 wt % in isopropanol), 2-butyl alcohol, and *N*,*N*-dimethylformamide (DMF, ≥99.9%) were from Sigma-Aldrich. Carbon paste was from Shanghai Materwin New Materials Co., Ltd.

2.2. Device Fabrication

FTO glass (7 Ω sq^{-1}) was cleaned with deionized water, ethanol, and IPA. Titanium diisopropoxide bis(acetylacetonate) was diluted by 2-butyl alcohol before deposition on the UV−ozone-treated FTO substrate by spin-coating at 3000 rpm for 30 s. The fabricated substrates were annealed at 125 °C for 10 min in air. Subsequently, a mesoporous TiO_2 layer was deposited by spin-coating a commercial TiO_2 paste (Dyesol 30NRD), which was dispersed in ethanol (150 mg/mL), at 4000 rpm for 10 s. The films were subjected to a two-step thermal treatment: first drying at 120 °C for 10 min, followed by annealing at 500 °C for 30 min. The $CsPbI_3$ precursor solution (1.0 M) was prepared by dissolving 259.71 mg of CsI, 694.5 mg of PbI_2, and 259.9 mg of DMAI in 1000 μL of DMF and was spin-coated on TiO_2 at 2000 rpm for 20 s. The film was quickly placed on a hot plate at a temperature of 230 °C for 5 min. For ES modification, 0, 0.5, 1, and 1.5 mg/mL ES were dissolved in IPA. The film was spin-coated at 2000 rpm for 20 s and subsequently annealed at 100 °C for 5 min. The carbon electrode was prepared by depositing carbon paste through a doctor-blade coating, followed by drying at 120 °C for 15 min.

3. RESULTS AND DISCUSSION

To construct efficient and stable $CsPbI_3$ C-IPSCs, ES is introduced as an effective passivator onto the perovskite surface. The corresponding preparation process of the ES-treated $CsPbI_3$ perovskite film is displayed in Figure 1a. After

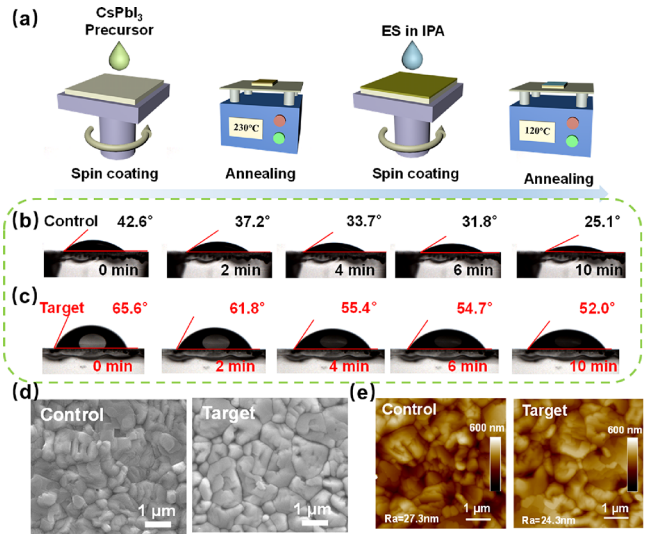

Figure 1. (a) Preparation process of an ES-treated $CsPbI_3$ perovskite film. Temporal evolution of CA for the (b) control and (c) target perovskite films. SEM (d) and AFM (e) images of the control and target perovskite films.

annealing the perovskite film, ES solutions of different concentrations (dissolved in IPA) were spin-coated onto the perovskite surface, followed by annealing at 120 °C for 5 min to achieve efficient surface passivation. The detailed preparation process is depicted in the Supporting Information. We first characterized the water contact angle (CA) of $CsPbI_3$ perovskite films with and without ES treatment, as shown in Figure 1b,c. The measured CA for the control perovskite film was 42.6°. As the contact time extended to 10 min, the CA rapidly decreased to 25.1°, representing a reduction of ∼41%. In contrast, the initial CA of the target perovskite film increases to 65.6° and remains around 52° after 10 min, only decreasing by 21%. At the same time, in subsequent observations, the contact angle of the control film continued to decrease over time. In contrast, the contact angle of the ES-modified film remained stable between 10 and 20 min, with no significant changes observed (Figure S1). These results indicate that ES treatment can enhance the hydrophobicity of the $CsPbI_3$ perovskite films. High hydrophobicity can inhibit hydrolysis by creating a physical barrier at the source. At the same time, this hydrophobic molecule can also anchor itself to the defect sites of perovskite materials through coordination, effectively inhibiting ion migration, which is beneficial for improving their phase stability and enhancing the stability of C-IPSCs.[27−29]

Meanwhile, we also characterize the CA of the $CsPbI_3$ perovskite films treated with ethyl acetate (EA) (Figure S2, Supporting Information). The value is slightly larger than that of the control film and still far behind that of the target perovskite film. We attribute this phenomenon to the hydrogen bonding ability and molecular polarity differences between EA and ES. The oxygen atom in the ester group of EA molecules has high electronegativity and contains lone-pair electrons, which can form weak but effective hydrogen bonds with hydrogen atoms in water molecules, enhancing their ability to interact with water. Meanwhile, the oxygen in the ester group of ES molecules is replaced by sulfur atoms, which significantly

https://doi.org/10.1021/acsaem.5c04098
ACS Appl. Energy Mater. XXXX, XXX, XXX−XXX

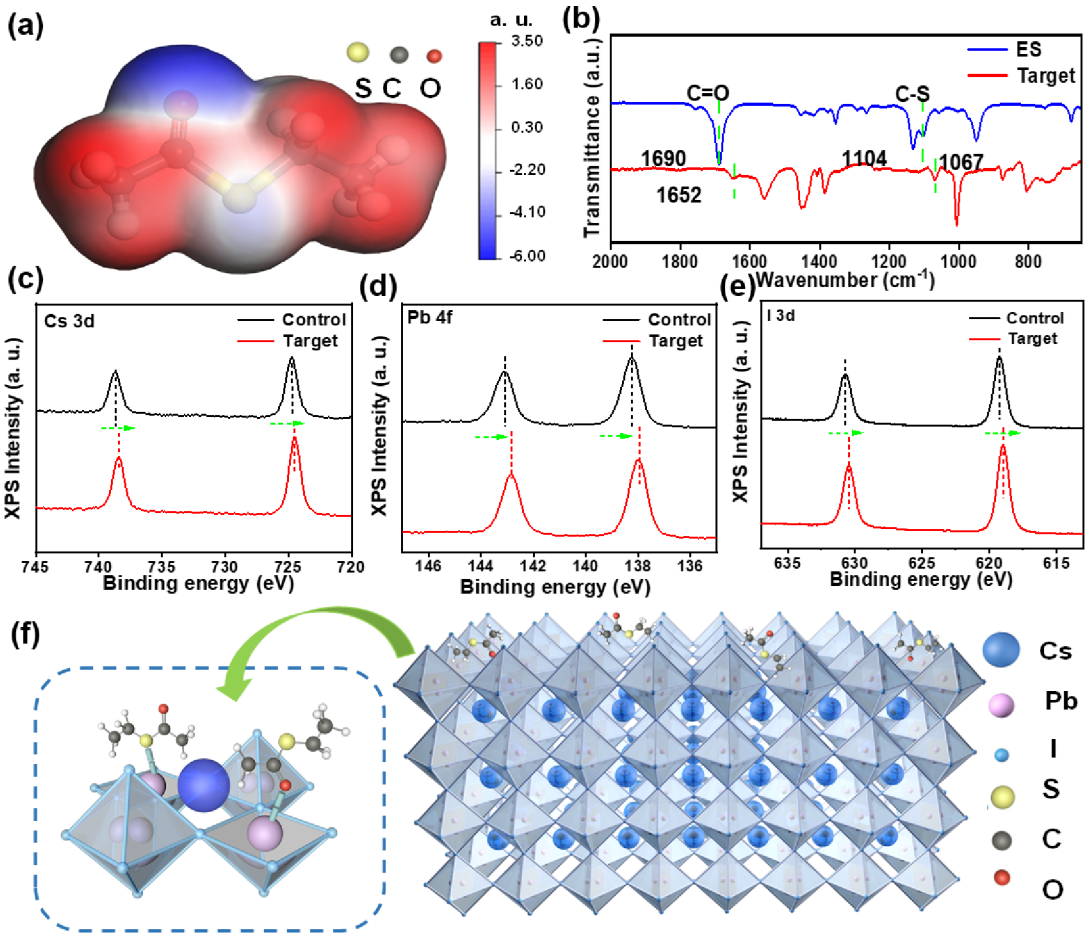

Figure 2. (a) Electrostatic potential of the ES. (b) FTIR spectra of ES and target perovskite films. XPS spectra of (c) Cs 3d, (d) Pb 4f, and (e) I 3d for the control and target perovskite films. (f) Proposed mechanism of the ES treatment for the $CsPbI_3$ perovskite film.

weakens the interaction with water. Also, the molecular polarity of EA is slightly higher than that of ES, resulting in the varied hydrophobicity.[30]

Focusing on the morphology of $CsPbI_3$ perovskite, scanning electron microscope (SEM) and atomic force microscope (AFM) measurements are conducted, as shown in Figure 1d,e. ES treatment increases the grain size from 1.09 to 1.34 μm and reduces their surface roughness to 24.3 nm, indicating its enhanced crystallinity and improved interface contact with carbon electrodes.[31−33] The SEM morphology of the sample after EA modification did not show significant changes compared to the standard sample (Figure S3). The X-ray diffraction (XRD) patterns are shown in Figure S4. The target perovskite film shows a more pronounced (110) diffraction peak at 14.28°, with a full width at half-maximum (fwhm) of 0.183. This value is smaller than the fwhm of the control film (0.197), indicating enhanced crystallinity in the target sample. Additionally, Figure S5 presents the ultraviolet−visible (UV−vis) absorption spectra of ES-modified films at various concentrations alongside the control film. The results show that the absorption intensities of the films remain largely unchanged. Tauc plots derived from the absorption data (Figure S6) indicate an optical band gap (E_g) of 1.72 eV both before and after ES modification, suggesting that ES treatment does not significantly alter the E_g of the inorganic perovskite.

Then, in order to study the chemical interaction between ES and $CsPbI_3$ perovskite films, the electrostatic potential (ESP) of the ES molecule is shown in Figure 2a; detailed computational methods are listed in the experimental section. The negative charge center mainly located near the C═O and S atoms, indicating that both sites tend to interact with the uncoordinated Pb^{2+} during surface defect passivation of the perovskite film.[34−36] Fourier transform infrared spectroscopy (FTIR) characterization is performed to further demonstrate the interaction conditions under ES treatment, as displayed in Figure 2b. For the ES molecule, the peaks at 1690 and 1104 cm^{-1} could be assigned to the C═O and C−S bond stretching vibration peaks, respectively. For the ES-treated perovskite film, the characteristic peaks shift to 1652 and 1067 cm^{-1}, indicating that C═O and C−S in the ES molecules interact with the inorganic perovskite, mainly coordinating with uncoordinated Pb^{2+}.

X-ray photoelectron spectroscopy (XPS) is conducted to characterize the Cs 3d, Pb 4f, and I 3d signal for the perovskite films with and without ES treatment, as shown in Figure 2c−e. Cs 3d, Pb 4f, and I 3d signal peaks shift to lower binding energies after ES passivation, indicating an increase in electron cloud density, which is caused by electron-rich C═O and C−S groups of ES that would interact with uncoordinated Pb^{2+}.[37−39] Based on the above analysis, Figure 2f illustrates that under ES molecular modification for inorganic perovskite films, the lone-pair electrons of C═O and C−S groups would interact with the uncoordinated Pb^{2+} on the surface of the $CsPbI_3$ perovskite and passivate the corresponding defects.

https://doi.org/10.1021/acsaem.5c04098
ACS Appl. Energy Mater. XXXX, XXX, XXX−XXX

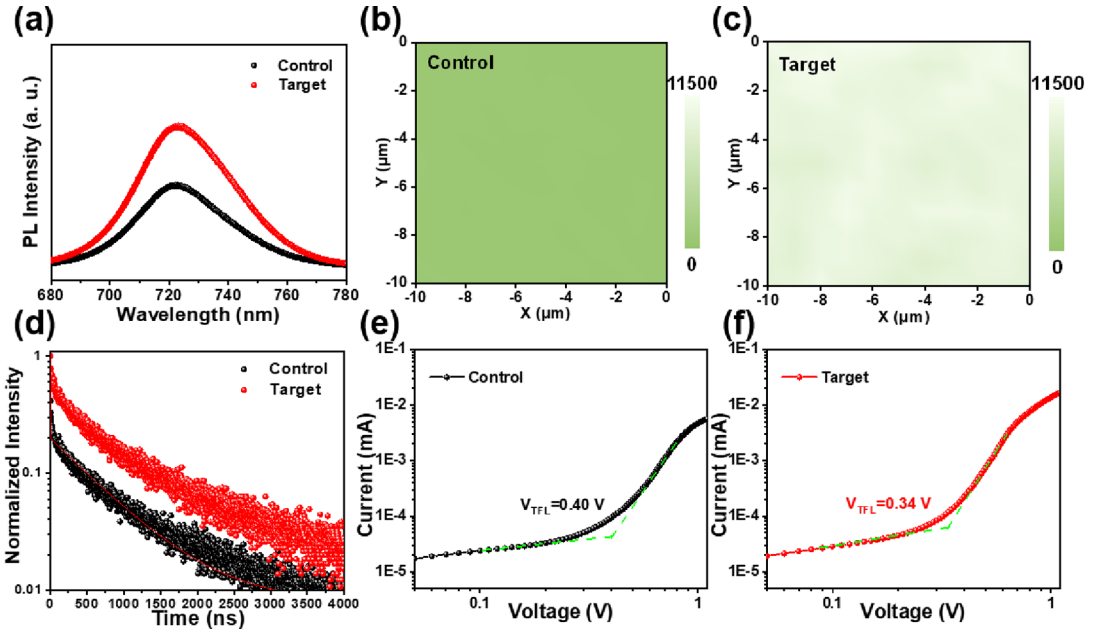

Figure 3. (a) PL spectra of the control and target perovskite films. PL mapping of (b) control and (c) target perovskite films. (d) TRPL curves of the control and target perovskite films. SCLC curves of electron-only devices: FTO/TiO_2/perovskite/PCBM/Ag based on (e) control and (f) target perovskite films.

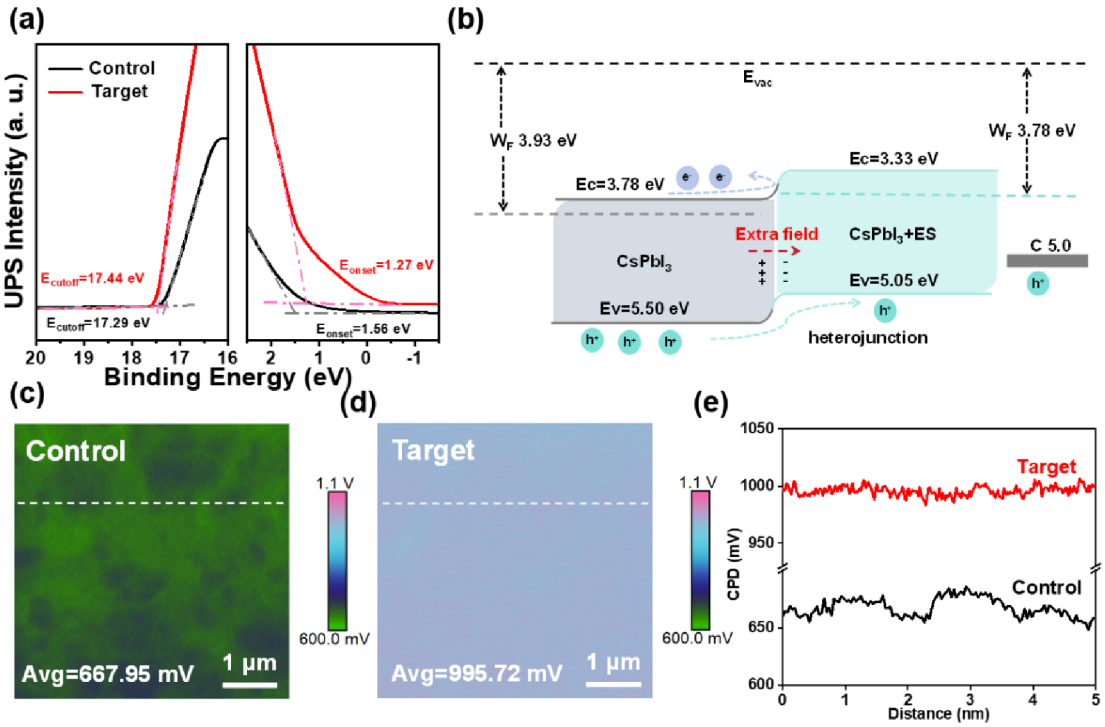

Figure 4. (a) UPS curves of the control and target perovskite films. (b) Schematic energy level arrangement. KPFM images of (c) control and (d) target perovskite films. (e) Horizontal distribution of surface potential along the marked lines in KPFM images.

Focusing on the defect density of $CsPbI_3$ perovskite films with and without ES treatment, steady-state photoluminescence (PL) spectroscopy is conducted, as displayed in Figure 3a. Both films show an emission peak at around 725 nm, corresponding to the intrinsic emission of $CsPbI_3$ perovskite. The enhanced intensity of the ES-treated perovskite film indicates the effectively reduced defect density of $CsPbI_3$ perovskite films.[40] Meanwhile, PL mapping is performed with a scanning range of 10 × 10 μm, as depicted in Figure 3b,c, demonstrating the overall enhanced PL intensity as well as reduced defect density for the ES-treated perovskite films. Subjecting the films on conductive substrates to ES modification resulted in a decrease in PL intensity (Figure S7), which suggests enhanced charge transfer efficiency. Time-resolved PL (TRPL) curves of the perovskite films on glass are compared, as shown in Figure 3d. From TRPL curves and corresponding fitting parameters of both samples (Table S1), we can see that the target perovskite film shows a greatly

https://doi.org/10.1021/acsaem.5c04098
ACS Appl. Energy Mater. XXXX, XXX, XXX−XXX

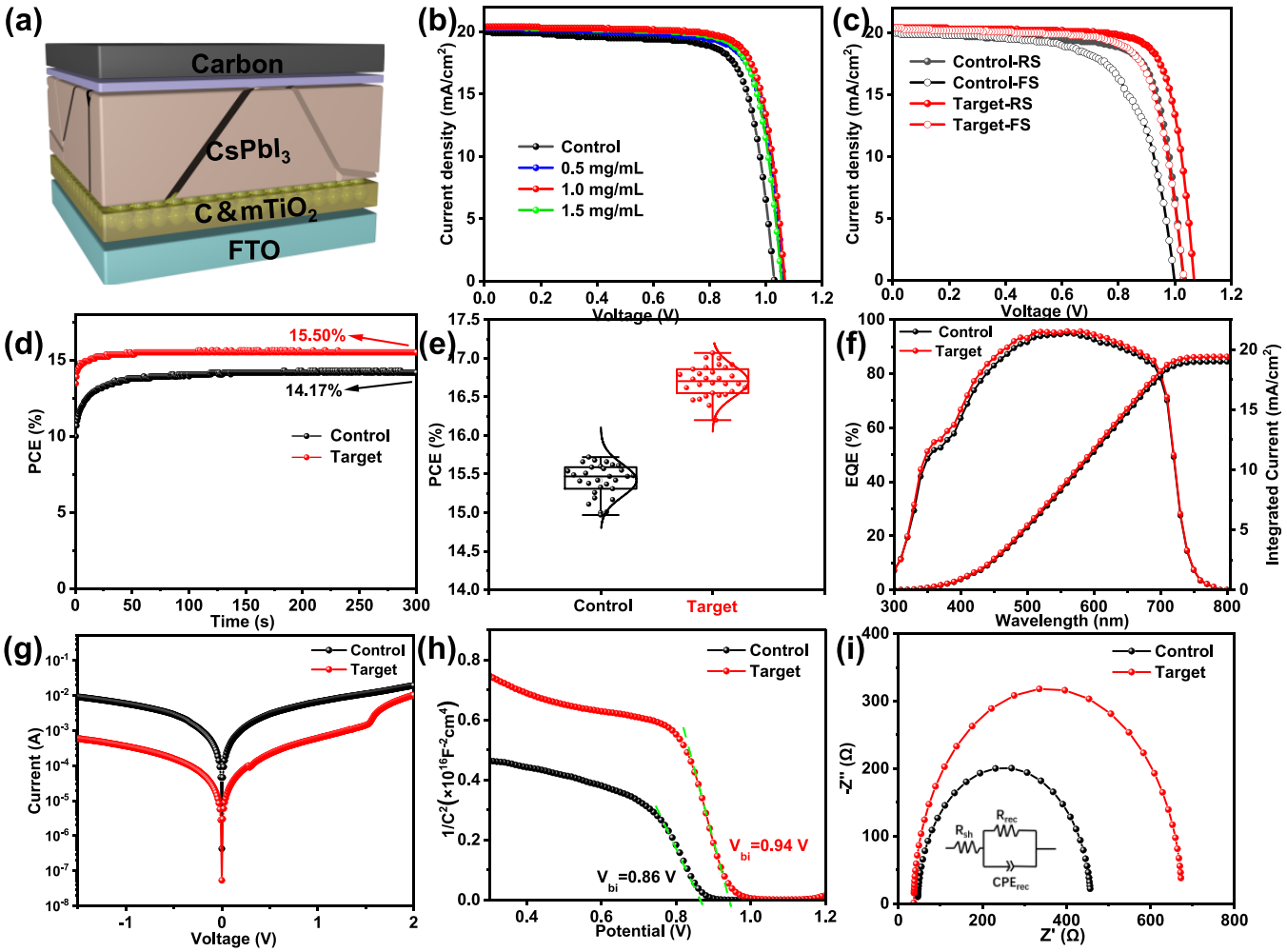

Figure 5. (a) Device structure of $CsPbI_3$ C-IPSCs. (b) $J-V$ curves of the C-IPSCs treated with different ES concentrations. (c) $J-V$ curves of the control and target C-IPSCs measured under RS and FS. (d) SPO curves, (e) statistical PCE distribution, (f) EQE curves, (g) dark $I-V$ curves, (h) M−S analysis, and (i) Nyquist plots of the control and target C-IPSCs.

enhanced PL lifetime (τ_{ave}) from 681.45 to 916.86 ns, further demonstrating the effective defect passivation ability of the ES molecule.

Furthermore, space charge limited current (SCLC) curves of both samples using electron-only devices (FTO/TiO_2/perovskite/PCBM/Ag) are depicted in Figure 3e,f. The estimated trap-filled limit voltage (V_{TFL}) declines from 0.40 to 0.34 V. According to the equation $N_t = 2\varepsilon\varepsilon_0 V_{TFL}/eL^2$, where N_t represents defect density, ε and L are the relative dielectric constant and thickness of perovskite film, respectively, ε_0 is the vacuum dielectric constant, and e is the electron charge, the target perovskite film shows decreased N_t values from 4.13×10^{14} to 3.31×10^{14} cm^{-3} after ES treatment, which is consistent with the PL and TRPL results.[41−43]

Apart from the reduced defect density for the ES post-treatment, ES modification could optimize the energy level arrangement at the perovskite/carbon interface as well. Ultraviolet photoelectron spectroscopy (UPS) is employed as shown in Figure 4a, from which the energy levels are calculated.[44] The target sample exhibits elevated Fermi levels (from −4.93 to −3.78 eV) as well as VBM values (from −5.50 to −5.05 eV) that are close to the energy level of the carbon electrode in Figure 4b and Figure S8, which could accelerate the hole extraction at the interface.[45] In addition, the tuned conduction band minimum of the target perovskite could further block the electron pass through perovskite to the carbon electrode, which can effectively reduce the leakage current, thereby enhancing device performance.[46−48]

Figure 4c,d corresponds to Kelvin probe force microscopy (KPFM) characterizations with surface potential distribution along the marked lines shown in Figure 4e. From the results, we can see that the average contact potential difference (CPD) of the target perovskite film exhibits a higher value (995.72 mV) than that of the control (667.95 mV), which is consistent with the UPS result. At the same time, as shown in the Figure S9 distribution map, the CPD of the control film fluctuates, with a scattered distribution, showing notable inhomogeneity. In contrast, the CPD distribution of the target film is more concentrated and uniform, suggesting that the ES treatment can effectively passivate defects of the perovskite surface and improve the uniformity of perovskite films.

Photovoltaic performances of FTO/TiO_2/$CsPbI_3$/carbon devices were evaluated, as illustrated in Figure 5a. The $J-V$ curves of the $CsPbI_3$ C-IPSCs treated with different ES concentrations (0.5, 1.0, and 1.5 mg/mL) are depicted in Figure 5b, and the detailed device performance parameters are listed in Table S2. As can be seen, the control C-IPSC obtains a PCE of 15.61% with a short-circuit current density (J_{SC}) of

https://doi.org/10.1021/acsaem.5c04098
ACS Appl. Energy Mater. XXXX, XXX, XXX−XXX

19.97 mA/cm^2, an open-circuit voltage (V_{OC}) of 1.03 V, and a fill factor (FF) of 75.86%. Under a 0.5 mg/mL ES concentration, the PCE of the corresponding device increases to 16.56%. The value further increases to 17.07% when the ES concentration increases to 1 mg/mL, with J_{SC}, V_{OC}, and FF of 20.42 mA/cm^2, 1.07 V, and 78.24%, respectively. While for 1.5 mg/mL ES treatment, a slightly decreased PCE of 16.81% is obtained, mainly due to the fact that excessively passivated molecules deposited on perovskite films inhibit hole transport in C-IPSCs. Thus, the 1 mg/mL ES concentration is selected as the optimal condition for $CsPbI_3$ C-IPSCs. Considering the hysteresis effect of C-IPSCs, Figure 5c depicts the $J-V$ curves measured under a reverse scan (RS) and a forward scan (FS), and the corresponding device performance parameters are listed in Table 1. According to the formula of the hysteresis index (HI) = $(PCE_{RS} - PCE_{FS})/PCE_{RS}$, the HI value of the target C-IPSC decreases from 0.15 to 0.09, further proving the effective defect passivation ability of the ES molecules.[49] This passivation strategy also performs effectively in devices prepared with Ag electrodes (Figure S10). Subsequently, we applied EA for film passivation in a carbon-based device architecture. The resulting optoelectronic performance parameters were largely comparable to those of the control group, with no significant differences observed (Figure S11).

Table 1. Device Performance Parameters of the Control and Target C-IPSCs Measured under RS and FS

sample	J_{SC} (mA/cm^2)	V_{OC} (V)	FF (%)	PCE (%)	HI
control-RS	19.97	1.03	75.86	15.61	0.15
control-FS	19.97	0.99	66.56	13.29	
with ES-RS	20.42	1.07	78.24	17.07	0.09
with ES-FS	20.41	1.03	74.36	15.62	

Figure 5d displays the stable power output (SPO) curves for the control and target C-IPSCs. We can see that the target device achieves a stable efficiency within 300 s. To demonstrate the reproducibility of the device performance, we collected a batch of control and target C-IPSCs (30 devices), and Figure 5e shows the statistical distribution of the PCE values, which further demonstrates the effectiveness of ES treatment for defect passivation. In addition, Figure 5f depicts the external quantum efficiency (EQE) spectrum and the integrated J_{SC} is estimated to be 19.00 and 19.42 mA/cm^2 for the control and target C-IPSCs, in accordance with the above $J-V$ results.[50−52]

Dark $I-V$ measurements are conducted for the control and target C-IPSCs and are shown in Figure 5g. The target device shows a reduced leakage current, indicating the inhibited photogenerated carrier shunting along the defect-assisted channels.[53] Mott−Schottky analysis is performed, and the built-in potential (V_{bi}) is estimated using the following equation: $1/C^2 = 2(V_{bi} - V)/A^2 e\varepsilon_0 \varepsilon N_A$, where C is the capacitance under applied voltage; ε_0 and ε are the vacuum dielectric constant and relative dielectric constant of the perovskite, respectively; and A, e, and N_A are the device area,

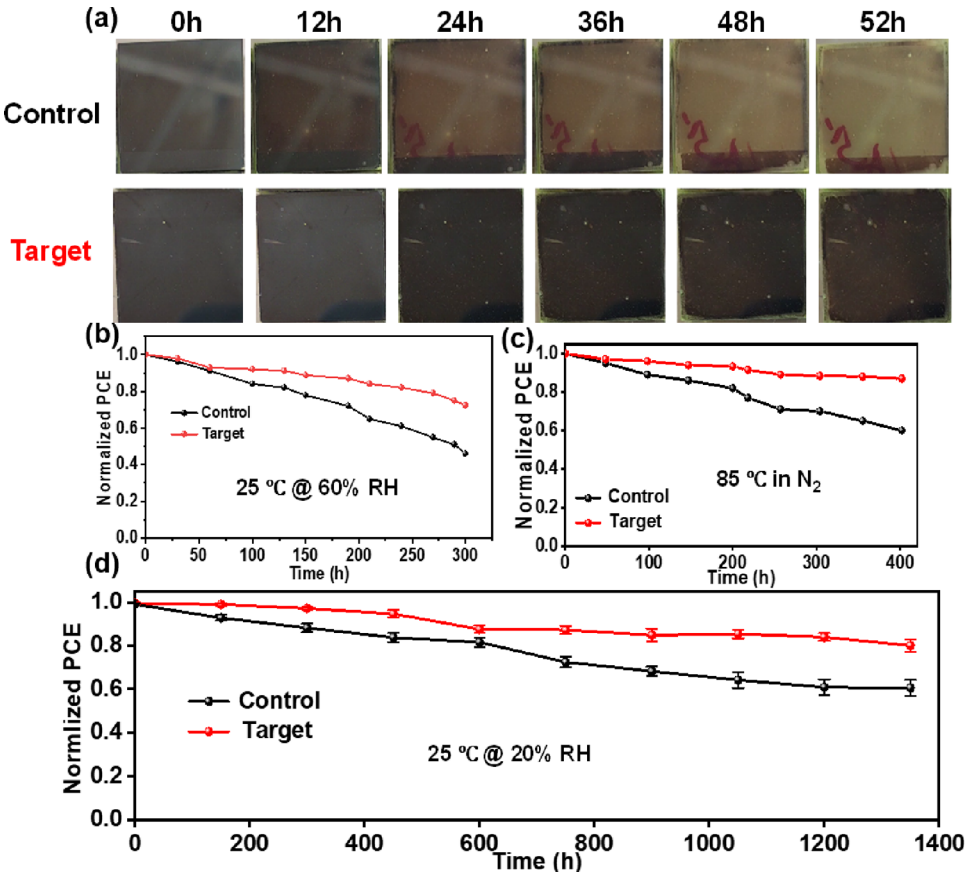

Figure 6. (a) Temporal evolution of control and target perovskite films under an ambient environment with an RH of 40−50%. (b) Humidity stability of devices under 25 °C with an RH of 60%. (c) Thermal stability of C-IPCSs under 85 °C in a N_2 atmosphere. (d) Long-term storage stability of C-IPSCs in ambient air with an RH of 20%.

https://doi.org/10.1021/acsaem.5c04098
ACS Appl. Energy Mater. XXXX, XXX, XXX−XXX

elementary charge, and carrier concentration, respectively.[54] Figure 5h indicates that the ES treatment increases the V_{bi} of the corresponding devices from 0.86 to 0.94 V, consistent with the increased V_{oc} values. The charge transfer and recombination process in C-IPSCs is investigated via electrochemical impedance spectroscopy (EIS) measurement with the typical Nyquist plots shown in Figure 5i. Figure S12 illustrates the corresponding equivalent circuit, and Table S3 lists the fitted results. The series resistance (R_s) decreased from 45.93 to 36.86 Ω for the target C-IPSCs, suggesting enhanced carrier transportation. The recombination resistance (R_{rec}) increases from 412.2 to 637.9 Ω for the target C-IPSCs. This increase in R_{rec} results from the suppressed carrier recombination and leads to an improved V_{OC} and FF.[55]

Long-term humidity and thermal and storage stabilities of the ES-modified $CsPbI_3$ C-PSCs have been measured, as shown in Figure 6. First, we trace the color change of the perovskite films under an RH of 40−50%, as displayed in Figure 6a. The color of the control perovskite film turns yellow after 24 h, and the target perovskite film remains black even after 52 h, indicating that ES modification can improve the humidity stability of the inorganic perovskite film, consistent with the CA measurement mentioned above. The humidity stability of the control and target C-IPSCs is shown in Figure 6b. The target C-IPSCs can maintain 72% of their initial efficiency after 300 h of storage under 25 °C with an RH of 60%, compared with 46% for the control C-IPSCs, further demonstrating that ES treatment can improve the humidity stability of $CsPbI_3$ perovskite films. Then, we also tested the thermal stability of C-IPSCs at 85 °C under a N_2 atmosphere, as displayed in Figure 6c. After 400 h of storage under 85 °C in N_2 conditions, the target PSCs maintain 87% of the initial PCE, mainly due to the improved phase stability and reduced defect density of the perovskite films. In addition, the long-term storage stability of C-IPSCs in air with an RH of 20% is also monitored, as shown in Figure 6d. After 1360 h of storage, the ES-treated device maintains 80% of the initial PCE, whereas the control device drops to 61%. ES post-treatment facilitates the formation of a hydrophobic surface to resist the external water damage. The C═O bond and S atoms in the ES could form effective coordination with the uncoordinated Pb^{2+} of the perovskite film, effectively passivating the defects and suppressing the degradation of the device during long-term operation.

4. CONCLUSIONS

In this work, a facile molecular modification strategy is proposed to fabricate $CsPbI_3$ C-IPSCs with high efficiency and stability. Post-treatment effectively improves the hydrophobicity of $CsPbI_3$ films due to the relatively small polarity of the ES molecules. Meanwhile, C═O and C−S in ES can form Lewis acid−base coordination interactions with uncoordinated Pb^{2+} in perovskite, effectively passivating surface defects in perovskite films. In addition, ES treatment optimizes energy level arrangement between inorganic perovskite and carbon electrodes, accelerating the hole extraction at the perovskite/carbon interface. Thus, ES post-treatment yields a champion PCE of 17.07%, which is among the high values for carbon-based $CsPbI_3$ cells. The ES-treated C-IPSCs also show enhanced stability, and the treated devices retain 80% of their initial PCE after 1360 h of storage at 20% RH, surpassing the untreated counterparts by 19%.

■ ASSOCIATED CONTENT

Supporting Information

The Supporting Information is available free of charge at https://pubs.acs.org/doi/10.1021/acsaem.5c04098.

Contact angle test of $CsPbI_3$ perovskite films with EA treatment, XRD patterns, Tauc plot, equivalent circuit model of control and target devices, fitting parameters of TRPL spectra, corresponding parameters of devices with different concentrations of ES, and fitted results of Nyquist plots of the control and target $CsPbI_3$ C-IPSCs (PDF)

■ AUTHOR INFORMATION

Corresponding Authors

Tingting You − *School of Chemistry, Beihang University, Beijing 100191, P. R China*; Email: youtt@buaa.edu.cn

Penggang Yin − *School of Chemistry, Beihang University, Beijing 100191, P. R China*; orcid.org/0000-0001-6796-5921; Email: pgyin@buaa.edu.cn

Authors

Zhixing Wang − *School of Chemistry, Beihang University, Beijing 100191, P. R China*

Jinqing Lv − *School of Chemistry, Beihang University, Beijing 100191, P. R China*

Weifeng Liu − *School of Chemistry, Beihang University, Beijing 100191, P. R China*

Weiwei Sun − *School of Chemistry, Beihang University, Beijing 100191, P. R China*

Zhiwen Dong − *School of Chemistry, Beihang University, Beijing 100191, P. R China*

Kexiang Wang − *School of Energy and Power Engineering, Beihang University, Beijing 100191, China*

Complete contact information is available at: https://pubs.acs.org/10.1021/acsaem.5c04098

Author Contributions

[1]Z.W. and J.L. contributed equally to this work. All authors have approved the final version of the manuscript.

Notes

The authors declare no competing financial interest.

■ ACKNOWLEDGMENTS

This work is financially supported by the National Natural Science Foundation of China (Nos. 62305015 and 22005013). The authors acknowledge the facilities and the scientific and technical assistance of the Analysis & Testing Center, Beihang University.

■ REFERENCES

(1) Xiong, Z.; Zhang, Q.; Cai, K.; Zhou, H.; Song, Q.; Han, Z.; Kang, S.; Li, Y.; Jiang, Q.; Zhang, X.; et al. Homogenized Chlorine Distribution for > 27% Power Conversion Efficiency in Perovskite Solar Cells. *Science* **2025**, *390* (6773), 638−642.

(2) Hu, S.; Otsuka, K.; Murdey, R.; Nakamura, T.; Truong, M. A.; Yamada, T.; Handa, T.; Matsuda, K.; Nakano, K.; Sato, A.; et al. Optimized Carrier Extraction at Interfaces for 23.6% Efficient Tin−Lead Perovskite Solar Cells. *Energy Environ. Sci.* **2022**, *15* (5), 2096−2107.

(3) Swarnkar, A.; Marshall, A. R.; Sanehira, E. M.; Chernomordik, B. D.; Moore, D. T.; Christians, J. A.; Chakrabarti, T.; Luther, J. M.

Quantum Dot-Induced Phase Stabilization of Alpha-$CsPbI_3$ Perovskite for High-Efficiency Photovoltaics. *Science* **2016**, *354* (6308), 92−95.
(4) McMeekin, D. P.; Sadoughi, G.; Rehman, W.; Eperon, G. E.; Saliba, M.; Horantner, M. T.; Haghighirad, A.; Sakai, N.; Korte, L.; Rech, B.; et al. A Mixed-Cation Lead Mixed-Halide Perovskite Absorber for Tandem Solar Cells. *Science* **2016**, *351* (6269), 151−155.
(5) Wang, Y.; Dar, M. I.; Ono, L. K.; Zhang, T.; Kan, M.; Li, Y.; Zhang, L.; Wang, X.; Yang, Y.; Gao, X.; et al. Thermodynamically Stabilized β-CsPbI3−based Perovskite Solar Cells with Efficiencies > 18%. *Science* **2019**, *365*, 591−595.
(6) Mei, A.; Li, X.; Liu, L.; Ku, Z.; Liu, T.; Rong, Y.; Xu, M.; Hu, M.; Chen, J.; Yang, Y.; et al. A Hole-Conductor-Free, Fully Printable Mesoscopic Perovskite Solar Cell with High Stability. *Science* **2014**, *345* (6194), 295−298.
(7) Zhang, Q.; Liu, H.; Wei, X.; Song, Y.; Lv, C.; Li, W.; Zhu, L.; Lan, Y.; Du, Y.; Wang, K.; Yin, P.; Lin, C.; Lin, Z.; Bai, Y.; Chen, Q.; Yang, S.; Chen, H.; et al. Deploying a Dipole Electric Field at the $CsPbI_3$ Perovskite/Carbon Interface for Enhancing Hole Extraction and Photovoltaic Performance. *Small* **2024**, No. e2402061.
(8) Rui, D.; Fu, J.; Chen, Q.; Cao, J.; Wu, W.; Chen, L.; Zhang, J.; Zhang, Z.; Zhou, Y.; Song, B. Surface Engineering Based on Ionic Liquids for Efficient and Stable $CsPbI_3$ Perovskite Solar Cells. *J. Mater. Chem. A* **2024**, *12* (13), 7847−7855.
(9) Liu, N.; Liu, Z.; Wang, J.; Ye, Q.; Wang, Y.; Han, W.; Xu, W.; Zhang, J.; Huang, L.; Hu, Z.; et al. Synchronous Surface Reconstruction and Grain Boundary Healing Toward Efficient and Stable Inverted $CsPbI_3$ Perovskite Solar Cells. *Chem. Eng. J.* **2024**, *485*, No. 149590.
(10) Zhang, G.; Zhang, J.; Yang, Z.; Pan, Z.; Rao, H.; Zhong, X. Role of Moisture and Oxygen in Defect Management and Orderly Oxidation Boosting Carbon-Based $CsPbI_2Br$ Solar Cells to a New Record Efficiency. *Adv. Mater.* **2022**, *34* (40), No. e2206222.
(11) Zhu, W.; Chai, W.; Chen, D.; Ma, J.; Chen, D.; Xi, H.; Zhang, J.; Zhang, C.; Hao, Y. High-Efficiency (>14%) and Air-Stable Carbon-Based, All-Inorganic CsPbI2Br Perovskite Solar Cells through a Top-Seeded Growth Strategy. *ACS Energy Lett.* **2021**, *6* (4), 1500−1510.
(12) Zhang, Z.; Ba, Y.; Chen, D.; Ma, J.; Zhu, W.; Xi, H.; Chen, D.; Zhang, J.; Zhang, C.; Hao, Y. Generic Water-Based Spray-Assisted Growth for Scalable High-Efficiency Carbon-Electrode All-Inorganic Perovskite Solar Cells. *iScience* **2021**, *24* (11), No. 103365.
(13) Zhou, Q.; Duan, J.; Du, J.; Guo, Q.; Zhang, Q.; Yang, X.; Duan, Y.; Tang, Q. Tailored Lattice "Tape" to Confine Tensile Interface for 11.08%-Efficiency All-Inorganic $CsPbBr_3$ Perovskite Solar Cell with an Ultrahigh Voltage of 1.702 V. *Adv. Sci.* **2021**, No. e2101418.
(14) Xiang, S.; Fu, Z.; Li, W.; Wei, Y.; Liu, J.; Liu, H.; Zhu, L.; Zhang, R.; Chen, H. Highly Air-Stable Carbon-Based α-$CsPbI_3$ Perovskite Solar Cells with a Broadened Optical Spectrum. *ACS Energy Lett.* **2018**, 3 (8), 1824−1831.
(15) Wang, H.; Liu, H.; Dong, Z.; Li, W.; Zhu, L.; Chen, H. Composition Manipulation Boosts the Efficiency of Carbon-Based $CsPbI_3$ Perovskite Solar Cells to Beyond 14%. *Nano Energy* **2021**, *84*, No. 105881.
(16) Zhang, Q.; Wu, Y.; Wei, X.; Li, G.; Lv, C.; Gao, M.; Li, W.; Zhu, L.; Lan, Y.; Wang, K.; Yin, P.; Bai, Y.; Zhu, C.; Chen, Q.; Liu, H.; Chen, H.; et al. Nano Space Confinement Crystal Growth Boosted Hole Extraction in Carbon Based $CsPbI_3$ Perovskite Solar Cells. *Adv. Funct. Mater.* **2024**, *35* (16), No. 2419709.
(17) Lü, J.; Huo, X.; Liu, W.; Sun, W.; Ji, S.; You, T.; Wang, K.; Lü, W.; Wang, S. Additive Engineering by Dicyandiamide for High-Performance Carbon-Based Inorganic Perovskite Solar Cells. *Mater. Today Energy* **2024**, *44*, No. 101628.
(18) Liu, Z.; Sun, B.; Liu, X.; Han, J.; Ye, H.; Shi, T.; Tang, Z.; Liao, G. Efficient Carbon-Based CsPbBr3 Inorganic Perovskite Solar Cells by Using Cu-Phthalocyanine as Hole Transport Material. *Nanomicro Lett.* **2018**, *10* (2), 34.
(19) Tong, G.; Chen, T.; Li, H.; Qiu, L.; Liu, Z.; Dang, Y.; Song, W.; Ono, L. K.; Jiang, Y.; Qi, Y. Phase Transition Induced Recrystallization and Low Surface Potential Barrier Leading to 10.91%-Efficient CsPbBr3 Perovskite Solar Cells. *Nano Energy* **2019**, *65*, No. 104015.
(20) Wang, K.; Sun, W.; Liu, W.; Huo, X.; Yin, R.; Liu, J.; Gao, Y.; You, T.; Yin, P. Mitigating Interfacial and Bulk Defects via Chlorine Modulation for HTL-Free All-Inorganic CsPbI2Br Carbon-Based Perovskite Solar Cells with Efficiency Over 14%. *Chem. Eng. J.* **2022**, *445*, No. 136781.
(21) Liu, J.; Zhu, L.; Xiang, S.; Wei, Y.; Xie, M.; Liu, H.; Li, W.; Chen, H. Growing High-Quality CsPbBr3 by Using Porous CsPb2Br5 as An Intermediate: A Promising Light Absorber in Carbon-Based Perovskite Solar Cells. *Sustainable Energy Fuels* **2019**, 3 (1), 184−194.
(22) Li, Y.; Duan, J.; Yuan, H.; Zhao, Y.; He, B.; Tang, Q. Lattice Modulation of Alkali Metal Cations Doped Cs1−xRxPbBr3 Halides for Inorganic Perovskite Solar Cells. *Sol. RRL* **2018**, *2* (10), No. 1800164.
(23) Gong, S.; Li, H.; Chen, Z.; Shou, C.; Huang, M.; Yang, S. CsPbI2Br Perovskite Solar Cells Based on Carbon Black-Containing Counter Electrodes. *ACS Appl. Mater. Interfaces* **2020**, *12* (31), 34882−34889.
(24) Tong, G.; Chen, T.; Li, H.; Song, W.; Chang, Y.; Liu, J.; Yu, L.; Xu, J.; Qi, Y.; Jiang, Y. High Efficient Hole Extraction and Stable All-Bromide Inorganic Perovskite Solar Cells via Derivative-Phase Gradient Bandgap Architecture. *Sol. RRL* **2019**, *3* (5), No. 1900030.
(25) Zhao, F.; Guo, Y.; Wang, X.; Tao, J.; Jiang, J.; Hu, Z.; Chu, J. Enhanced Performance of Carbon-Based Planar CsPbBr3 Perovskite Solar Cells with Room-Temperature Sputtered Nb2O5 Electron Transport Layer. *Sol. Energy* **2019**, *191*, 263−271.
(26) Zhang, J.; Zhang, G.; Su, P.; Huang, R.; Lin, J.; Wang, W.; Pan, Z.; Rao, H.; Zhong, X. 1D Choline-PbI_3-Based Heterostructure Boosts Efficiency and Stability of $CsPbI_3$ Perovskite Solar Cells. *Angew. Chem., Int. Ed.* **2023**, *62* (25), No. e202303486.
(27) Liu, X.; Zhang, J.; Wang, H.; Miao, Y.; Guo, T.; Ono, L. K.; Yuan, S.; Wang, Y.; Ji, P.; Chen, H.; et al. CsPbI3 Perovskite Solar Module With Certified Aperture Area Efficiency > 18% Based on Ambient-Moisture-Assisted Surface Hydrolysis. *Joule* **2024**, *8* (10), 2851−2862.
(28) Fu, Y.; Han, H.; Liu, H.; Xu, J.; Liu, Y.; Shi, R.; Yao, J. In Situ Formation Of An Inorganic Lead Oxysalt Surface Passivation Layer For Highly Efficient And Stable $CsPbI_3$ Perovskite Solar Cells. *J. Mater. Chem. A* **2024**, *12* (5), 2877−2886.
(29) Zhang, J.; Zhang, G.; Liao, Y.; Pan, Z.; Rao, H.; Zhong, X. Interfacial Energy-Level Alignment via Poly-3-hexylthiophene-$CsPbI_3$ Quantum Dots Hybrid Hole Conductor For Efficient Carbon-Based $CsPbI_2Br$ Solar Cells. *Chem. Eng. J.* **2023**, *453*, No. 139842.
(30) Li, X.; Zhang, W.; Guo, X.; Lu, C.; Wei, J.; Fang, J. Constructing Heterojunctions by Surface Sulfidation for Efficient Inverted Perovskite Solar Cells. *Science* **2022**, *375* (6579), 434−437.
(31) Wang, H.; Liu, H.; Dong, Z.; Wei, X.; Li, W.; Zhu, L.; Zhu, C.; Bai, Y.; Chen, H. Dimethyl sulfoxide: a promising solvent for inorganic $CsPbI_3$ perovskite. *Sci. Bull. (Beijing)* **2023**, *68* (2), 192−202.
(32) Yin, R.; Wang, K.; Huo, X.; Sun, Y.; Sun, W.; Gao, Y.; You, T.; Yin, P. A One-Step Ionic Liquid Interface-to-Bulk Modification for Stable Carbon-Based $CsPbI_3$ Perovskite Solar Cells with Efficiency Over 15%. *Adv. Mater. Interfaces* **2022**, *9* (29), No. 2201488.
(33) Wang, H.; Liu, H.; Dong, Z.; Wei, X.; Song, Y.; Li, W.; Zhu, L.; Bai, Y.; Chen, H. Extracting Ammonium Halides by Solvent From the Hybrid Perovskites with Various Dimensions to Promote the Crystallization of $CsPbI_3$ Perovskite. *Nano Energy* **2022**, *94*, No. 106925.
(34) Zhang, Z.; Feng, Y.; Ding, J.; Ma, Q.; Zhang, H.; Zhang, J.; Li, M.; Geng, T.; Gao, W.; Wang, Y.; Zhang, B.; Pauporté, T.; Tang, J. X.; Chen, H.; Chen, J.; Chen, C.; et al. Rationally Designed Universal Passivator for High-Performance Single-Junction and Tandem Perovskite Solar Cells. *Nat. Commun.* **2025**, *16* (1), 753.
(35) Lin, J.; Huang, R.; Peng, X.; Zhang, J.; Zhang, G.; Wang, W.; Pan, Z.; Rao, H.; Zhong, X. Eliminating Hole Extraction Barrier in 1D/3D Perovskite Heterojunction for Efficient and Stable Carbon-

https://doi.org/10.1021/acsaem.5c04098
ACS Appl. Energy Mater. XXXX, XXX, XXX−XXX

Based $CsPbI_3$ Solar Cells with a Record Efficiency. *Adv. Mater.* **2024**, *36* (33), No. e2404561.
(36) Liu, C.; Zuo, C.; Xue, Q.; Lin, D.; Liu, T.; Luo, J.; Huang, H.; Chen, K.; Gao, Y.; Zeng, J.; Zhang, Y.; Xu, B.; Yang, T.; Mai, Y.; Zou, B.; Brabec, C. J.; Hu, X.; et al. Dimensional Regulation of Organic n-Type Dopants for Highly Efficient Perovskite Solar Cells and Modules. *Adv. Mater.* **2025**, *37* (10), No. e2417251.
(37) Tian, J.; Xue, Q.; Tang, X.; Chen, Y.; Li, N.; Hu, Z.; Shi, T.; Wang, X.; Huang, F.; Brabec, C. J.; Yip, H.; Cao, Y.; et al. Dual Interfacial Design for Efficient $CsPbI_2Br$ Perovskite Solar Cells with Improved Photostability. *Adv. Mater.* **2019**, *31* (23), No. e1901152.
(38) Wang, Q.; Chen, Y.; Chen, X.; Tang, W.; Qiu, W.; Xu, X.; Wu, Y.; Peng, Q. Tailored Succinic Acid-Derived Molecular Structures toward 25.41%-Efficiency and Stable Perovskite Solar Cells. *Adv. Mater.* **2024**, *36* (6), No. e2307709.
(39) Liu, C.; Yang, Y.; Chen, H.; Xu, J.; Liu, A.; Bati, A. S. R.; Zhu, H.; Grater, L.; Hadke, S. S.; Huang, C.; et al. Bimolecularly Passivated Interface Enables Efficient and Stable Inverted Perovskite Solar Cells. *Science* **2023**, *382* (6672), 810−815.
(40) Li, T.; Wang, K.; Tong, Y.; Qi, H.; Yue, S.; Li, W.; Wang, H. In Situ Dehydration Condensation of Self-Assembled Molecules Enables Stabilization of $CsPbI_3$ Perovskites for Efficient Photovoltaics. *Adv. Funct. Mater.* **2024**, *34*, No. 2409621.
(41) Li, R.; Zhang, S.; Zhang, H.; Wang, Z.; Feng, X.; Du, Y.; Zhou, T.; Chen, X.; Liu, P.; Liu, L.; Zhang, J.; Chen, Q.; Xi, L.; Zhao, K.; Liu, S. (.; Tian, Q.; et al. Customizing Aniline-Derived Molecular Structures to Attain beyond 22% Efficient Inorganic Perovskite Solar Cells. *Angew. Chem., Int. Ed. Engl.* **2024**, No. e202410600.
(42) Guo, X.; Lu, C.; Zhang, W.; Yuan, H.; Yang, H.; Liu, A.; Cui, Z.; Li, W.; Hu, Y.; Li, X.; et al. In Situ Surface Sulfidation of $CsPbI_3$ for Inverted Perovskite Solar Cells. *ACS Energy Lett.* **2024**, *9* (1), 329−335.
(43) Zhang, H.; Tian, Q.; Xiang, W.; Du, Y.; Wang, Z.; Liu, Y.; Liu, L.; Yang, T.; Wu, H.; Nie, T.; Huang, W.; Najar, A.; Liu, S. (.; et al. Tailored Cysteine-Derived Molecular Structures towards Efficient and Stable Inorganic Perovskite Solar Cells. *Adv. Mater.* **2023**, *35* (31), No. e2301140.
(44) Zhuang, Q.; Xu, Z.; Li, H.; Zhang, C.; Gong, C.; Wang, H.; Li, X.; Zang, Z. Molecular Polymerization Strategy for Stable Perovskite Solar Cells with Low Lead Leakage. *Sci. Adv.* **2025**, *11* (19), No. eado7318.
(45) Zhou, J.; Luo, Y.; Li, R.; Tian, L.; Zhao, K.; Shen, J.; Jin, D.; Peng, Z.; Yao, L.; Zhang, L.; et al. Molecular Contacts with an Orthogonal Pi-skeleton Induce Amorphization to Enhance Perovskite Solar Cell Performance. *Nat. Chem.* **2025**, *17* (4), 564−570.
(46) Tan, S.; Tan, C.; Cui, Y.; Yu, B.; Li, Y.; Wu, H.; Shi, J.; Luo, Y.; Li, D.; Meng, Q. Constructing Interfacial Gradient Heterostructure Enables Efficient $CsPbI_3$ Perovskite Solar Cells and Printed Minimodules. *Adv. Mater.* **2023**, *35* (128), No. e2301879.
(47) Shen, H.; Li, X.; Zhang, X.; Zhou, H.; Zhang, H.; Liu, X.; Zhang, M.; Wu, J.; Xiang, Z.; Fang, W. Constructing Gradient Structure to Increase Efficiency for Carbon-Based Hole Transport Layer Free All-Inorganic Perovskite Solar Cells Using SCAPS-1D. *Sol. Energy* **2023**, *253*, 240−249.
(48) Qiu, J.; Zhou, Q.; Yu, M.; Liu, J.; Zhuang, R.; Hua, Y.; Ding, L.; Zhang, X. Modulating $CsPbI_3$ Crystallization by Using Diammonium Agent for Efficient Solar Cells. *SusMater.* **2023**, *3* (6), 894−908.
(49) Jiang, Y.; Xu, T.-F.; Du, H.-Q.; Rothmann, M. U.; Yin, Z.-W.; Yuan, Y.; Xiang, W.-C.; Hu, Z.-Y.; Liang, G.-J.; Liu, S. Z.; et al. Organic-inorganic Hybrid Nature Enables Efficient and Stable $CsPbI_3$-based Perovskite Solar Cells. *Joule* **2023**, *7* (12), 2905−2922.
(50) Wang, K.; Yin, R.; Sun, W.; Huo, X.; Liu, J.; Gao, Y.; You, T.; Yin, P. In Situ Constructing Intermediate Energy-Level Perovskite Transition Layer for 15.03% Efficiency HTL-Free Carbon-Based Perovskite Solar Cells with a High Fill Factor of 0.81. *Sol. RRL* **2021**, *6* (1), No. 2100647.
(51) Liu, W.; Sun, W.; Wang, K.; Xu, H.; Huo, X.; Yin, R.; Sun, Y.; Ji, S.; You, T.; Li, W.; et al. Surface Passivation of CsPbI3 Films for Efficient and Stable Hole-Transporting Layer-Free Carbon-Based Perovskite Solar Cells. *ACS Appl. Energy Mater.* **2023**, *6* (6), 3495−3503.
(52) Tan, X.; Wang, S.; Zhang, Q.; Liu, H.; Li, W.; Zhu, L.; Chen, H. Stabilizing $CsPbI_3$ Perovskite for Photovoltaic Applications. *Matter* **2023**, *6* (3), 691−727.
(53) Wang, H.; Liu, H.; Dong, Z.; Wei, X.; Li, W.; Zhu, L.; Zhu, C.; Bai, Y.; Chen, H. Moisture is Not Always Bad: H2O Accelerates the Conversion of DMAPbI3 Intermediate to CsPbI3 for Boosting the Efficiency of Carbon-based Perovskite Solar Cells to over 16%. *Fundam. Res.* **2024**, *4* (5), 1110−1117.
(54) Gao, M.; Ou, Z.; Wang, C.; Liu, L.; Hu, D.; Wan, W.; Chen, P.; Pan, Y.; Nie, S.; Luo, Y.; Zhang, P.; Peng, D.; Zhao, K.; Fu, M.; Liu, W.; Wang, X.; Zhang, W.; Guo, H.; Zheng, Y.; Xiao, Z.; Gao, X.; Ma, Z.; Wang, R.; Jiang, T.; Sun, K.; et al. Multifunctional Buried Molecule-Bridge for High-Performance Inverted Perovskite Solar Cells. *Adv. Mater.* **2025**, No. e14273.
(55) Dong, H.; Qu, J.; Yue, X.; Zhao, Y.; Wang, W.; Chen, D.; Zhu, W.; Xi, H.; Zhou, L.; Zhang, J.; Lu, G.; Zhang, C.; Hao, Y.; et al. Regulating the Perovskite Crystallization Dynamics Via Dual Modulation Strategy for Performance Enhancement of Perovskite Solar Cells. *Adv. Energy Mater.* **2024**, *15* (13), No. 2403965.

https://doi.org/10.1021/acsaem.5c04098
ACS Appl. Energy Mater. XXXX, XXX, XXX−XXX